Automated determination of patient setup errors in radiation therapy using spherical radio-opaque markers

Kwok Leung Lam, Randall K. Ten Haken, Daniel L. McShan, and Allan F. Thornton, Jr.
Department of Radiation Oncology, University of Michigan Medical Center, Ann Arbor, Michigan 48109-0010

(Received 1 June 1992; accepted for publication 19 March 1993)

Patient positioning accuracy can be quantified by the three-dimensional (3-D) translations and rotations required to transform the patient back to the desired position. Results of the current study show that the translations and rotations could be obtained from two projection images obtained radiographically on a linear accelerator when spherical radio-opaque markers were implanted inside or affixed to the surface of a skull phantom. In the study, films used to record the images were converted into digital gray scale images using a laser film digitizer. The marker images were located automatically by the computer using image processing techniques. By combining information from both projections, the 3-D locations of the markers were determined to submillimeter precision. Pairs of films were also analyzed for the phantom displaced from its original location by known amounts. The accuracy of the computed translations and rotations required for realignment of the phantom were found to be better than 1 mm and 0.3°, respectively; comparable to the accuracy of the readout system of the equipment used. The general methodology could be coupled with an electronic portal imaging device for use in computer aided or automated correction of patient position in radiotherapy.

Key words: radiotherapy localization, image processing, portal image

I. INTRODUCTION

Requirements for patient positioning accuracy increase when treatment fields are more conformal to the target. This is especially important when three-dimensional (3-D) noncoplanar fields are employed. Manual correction of patient setup errors is sometimes necessary, even when immobilization devices and laser alignment systems are used. The detection of setup errors depends on the visualization of anatomic landmarks. Corrective action depends on the 3-D perception of the technologist to determine the rotation and translation of the patient necessary for the realignment. Although numerous efforts have been made to quantify setup errors from portal images,[1–6] straightforward solutions for patient realignment are not readily obtained because a portal image is a two-dimensional projection of a 3-D patient.

Methods to determine 3-D anatomy from a small number of projection images have not been fully developed. Recently, methods for determining patient setup errors using radio-opaque markers affixed to the patient, instead of anatomical landmarks, have been proposed.[7,8] Images of radio-opaque markers have previously been used to register image sets,[9] but their utility in automated detection of patient setup error has not been studied. The 3-D spatial location of the markers (whether spherical or linear) can be determined from two projections. Patient setup error, and hence movements required for patient realignment, can then be quantified by the 3-D spatial translation and rotation of the markers necessary to bring them back to the standard location. As the correction is known and can be completed in one step, numerous trials and errors to bring the patient to the desired position can be avoided. This is especially important when patient position is localized for every treatment, as the exposure from taking multiple repeat images could be significant.

To make daily localization practical in a clinical setting, the process should be automated so that minimal operator input is needed. We have developed two algorithms to automate the process. The first algorithm is a general one, which locates marker images on a pair of projection films and computes the 3-D locations of the markers. It is used to determine the 3-D locations of the markers on the first fraction of treatment. The second algorithm is a specific algorithm that locates marker images on a pair of projection films by comparing them with a reference pair of projection films, such as the pair obtained on the first fraction. It is used to determine the 3-D locations of the markers on subsequent fractions of treatment. As the projection films on the first fraction and subsequent fractions are very similar, even if there are setup differences, information on the reference films (such as shape, size, contrast, and locations of marker images) can be exploited to facilitate the automatic detection of marker images.

In this study, images of spherical radio-opaque markers affixed to a skull phantom are analyzed with computer algorithms. The effectiveness of using image processing techniques to automatically locate the marker images is evaluated. The precision in locating the markers in three dimensions is determined, and the accuracy of the system to estimate translations and rotations of the skull phantom, purposely misaligned from its nominal position, is quantified.

 0094-2405/93/20(4)/1145/8/$1.20 © 1993 Am. Assoc. Phys. Med.

II. METHODS AND MATERIALS

A. Experimental methods

Fourteen tungsten carbide 2.4 mm diam ball bearing blanks were affixed to a skull phantom. Eight of them were inside the brain (implanted markers) and six of them were on the surface (surface markers) of the phantom (Fig. 1). The implanted markers were placed at the corners of a parallelepiped. For the surface markers; one was over the frontal bone, one was at the entrance of the left nostril, two were at the left and right external auditory meatuses, and two were at the left and right lateral canthi.

The phantom was affixed to a platform that could be rolled and tilted. The platform was then placed on the patient treatment couch of a Varian Clinac 2100 C linear accelerator (which could be translated and rotated). Thus the location and orientation of the phantom could be adjusted in the six degrees of freedom of a rigid body. The resolution of the vertical and the longitudinal readouts for couch motion was 1 mm. Lateral motion was measured with a ruler with millimeter divisions. The resolution of the readout for rotation angle of the patient treatment couch was 0.1°. The roll and tilt of the platform were set with a protractor level, which had divisions of 0.5°.

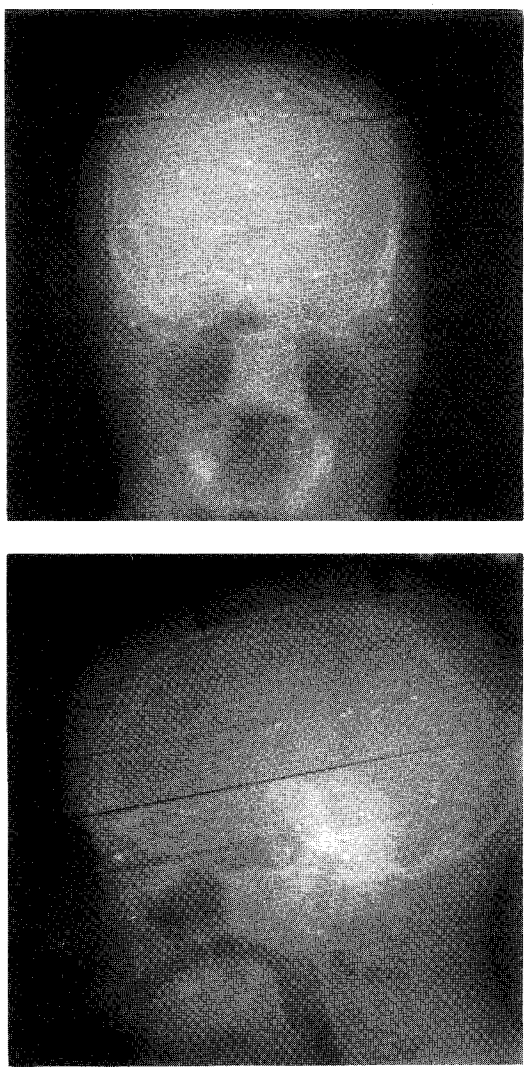

FIG. 1. A sample pair of orthogonal films on the skull phantom with 14 markers affixed to it. Air gaps between slices of the phantom show up as high optical density lines on the films. Two of the marker images overlap on the lateral film.

Orthogonal, anterior–posterior, and lateral localization films (Kodak T-MAT G films in Kodak localization cassettes) were taken (6 MV beam, Clinac 2100 C accelerator) at a reference position by rotating the gantry between exposures (Fig. 1). Although the projections do not need to be orthogonal for the computations, acquisition of orthogonal projections was found to be more convenient and reproducible. Subsequently, the phantom was either translated or rotated by known amounts, and film projections were taken at the same gantry angles. A total of 27 pairs of films were taken.

The films were digitized with a scanning laser film digitizer (Lumisys DIS 1000) with a laser beam spot size of 0.21 mm. Each pixel of the film was digitized to 12 bits with an optical density resolution of 0.001. The pixel spacing in the horizontal and vertical directions was 0.42 mm. The edges of the radiation field on the film images were determined as 50% of the maximum optical density. The coordinate system on the film was taken to be parallel to the field edges, with the origin at the center of the field.

B. Method of analysis for films at reference position

The method employed to locate marker images on the film was a simplification of the method used in the detection of microcalcifications in mammograms.[10] There were four steps in the image processing: gray scale transformation, linear filtering, gray scale thresholding, and signal extraction.

Optical density is approximately proportional to dose when a metal screen cassette is employed. As a result, the *percentage* decrease in optical density is equal to the *percentage* decrease in dose behind the marker. For a given percentage decrease in optical density, the magnitude of the decrease in optical density (which is defined as contrast) is larger in regions of higher optical density on the film. Logarithmic gray scale transform was performed on the digitized optical densities in order to keep the contrast more uniform from region to region; a technique used in Digital Subtraction Angiography[11] (See the Appendix).

As the marker images were more uniform than microcalcifications in terms of size, shape, and contrast, a conventional match filter[12] (matched to the circular marker image) was employed instead of the more complicated linear filter used by Chan *et al.*[10] Image features with a circular component were enhanced, and those without such a component were suppressed.

After linear filtering, skeletal features of the skull phantom were suppressed, so that their gray levels were different from that of the marker images. They were then effectively removed by using a gray scale window of one and gray scale level at the threshold level (gray scale thresholding[12]), so that the processed images have pixels of either black or white.

Potential marker images (regions of contiguous white pixels) were then searched for within the radiation field and checked for size and eccentricity. Images too large or too small in area were rejected. The location of a circular marker image was taken to be the centroid of its boundary. For a marker image that had a major axis larger than its minor axis by two pixels or more, two partially overlapping images were assumed. The locations of the two marker images were then assumed to be along the major axis of the composite image and at half the length of the minor axis from the two ends.

This general marker recognition algorithm was tested on all the film pairs obtained in the experiment (instead of just the original reference film pair) to provide more data. The marker images of the two projections at the reference position were matched and the 3-D marker locations were determined according to the two film technique used in brachytherapy source localization.[13]

C. Method of analysis for films from subsequent treatments

The determination of the 3-D location of the markers consists of two steps: the localization of marker images on the two projections and the computation of 3-D locations of markers from the locations of marker images. The algorithm is schematically illustrated in Fig. 2. Three major aspects of the information available from the reference film pairs were utilized: (1) the shape and contrast of the marker images on the reference film pair could be extracted and used as a template to locate marker images; (2) the algorithm only needed to search small regions around the locations of reference film marker images for marker images on the two projections; (3) the known relative 3-D positions of the markers can be used as a template to reject wrong matching of marker images from the two projections.

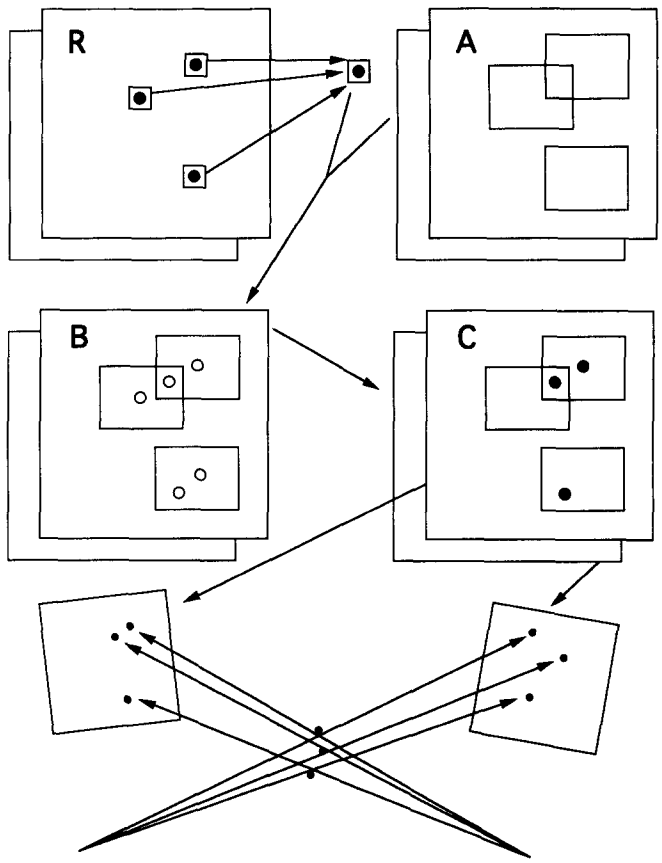

FIG. 2. Schematic diagram for the specific algorithm used in analyzing a portal image pair (A) with respect to a reference image pair (R). A template of the marker image was generated from R and regions of interest (ROI's, shown as rectangles on A) for potential marker images were delineated in A centered around corresponding marker locations in R. Image pair A was processed to give image pair B with potential marker image locations. Potential marker images were examined, and each ROI was assigned one potential marker image to form image pair C. Rays between the x-ray sources and the marker images were then constructed in 3-D space and potential locations of markers at the closest approach of the rays from the two projections were determined. The matching of rays that gave a 3-D structure of marker arrangement most similar to the 3-D structure of the markers from the reference image pair was taken to be the correct matching. The translation and rotation of the reference markers to these markers in 3-D space were then determined.

1. Localization of marker images on subsequent film pairs

A template of the marker image was generated from the reference films. Square 11×11 pixel arrays were extracted around each identified marker image. In order to minimize the effect of the average optical density around the marker images on the template, two image processing steps were performed on each of those 11×11 arrays: (1) a logarithmic gray scale transformation was performed; and (2) the average of the 121 array elements was subtracted from each array element. The template array was then obtained by taking the average of corresponding elements of this set of processed arrays.

The locations of potential marker images on subsequent treatment films were determined. Regions of interest (ROI's) of 4.2 cm by 4.2 cm were identified around the locations of marker images of the reference films. This assumed that the marker images did not move outside a 4.2 cm square from their locations on the reference film. Within each region, the following procedure was performed to identify potential marker images.

A correlation function[12] between the template array and the region was computed. It was defined as

$$r(m,n)=\frac{\Sigma_{j=1}^{11}\Sigma_{i=1}^{11}T(i,j)F(i+m,j+n)}{\{[\Sigma_{j=1}^{11}\Sigma_{i=1}^{11}T^2(i,j)][\Sigma_{j=1}^{11}\Sigma_{i=1}^{11}F^2(i+m,j+n)]\}^{1/2}},\quad \text{for } m,n=0,\ldots,90, \tag{1}$$

where $T(i,j)$ was the template and $F(i,j)$ was a 4.2 cm by 4.2 cm region.

The position of the maximum of the correlation function was taken as the location of a potential marker image if the correlation function was larger than 0.5, and the contrast was at least 0.5 of that of the template. The potential marker image was then removed from the region by subtracting the template array from the location found. The procedure of calculating a correlation function was then repeated until either the maximum of the correlation function or the contrast relative to that of the template dropped below 0.5. A set of potential marker image locations were then determined for each region.

Since the 4.2 cm by 4.2 cm regions might overlap, a potential marker image in an overlapping area would be identified as belonging to more than one region. Therefore, the potential marker image locations were sorted into distinct locations using an equivalence classes algorithm.[14] If any two potential marker images were at the same location, they were taken to be the same marker image.

Since the number of potential marker images found can be more than the number of regions and some potential marker images may belong to more than one region, a method is needed to assign a marker image to each region. We utilized the value of the correlation function of the potential marker images when they were identified to construct a cost function. If r_i was the value of the correlation function of potential marker image i, the cost function C was defined to be $C=(1-r_1)+(1-r_2)+\cdots+(1-r_n)$, where n is the number of regions. Each region was assigned only one of the distinct marker images within itself by minimizing the cost function with an algorithm for the square assignment problem.[13]

2. 3-D position of markers

On each of the two projections, n marker images were located. The problem was to match, for each marker image on projection 1, the corresponding marker image on projection 2. This is the same problem as two film brachytherapy source localization. For each marker image on the two projections, we computed the rays joining the x-ray source and that marker image in 3-D space. For each marker image on projection 1, we checked the shortest distance between its ray and the ray of each marker on projection 2. If the shortest distance was less than 2 mm between the rays, that marker image on projection 2 was taken as a candidate for matching the marker image on projection 1. After this procedure, each marker image on projection 1 had a set of matching marker images on projection 2. It is unlikely, although possible, that the rays from different marker images will approach each other within 2 mm, even if the marker images are projected from different markers. Therefore, these sets very rarely have more than two elements and most have only one. By the same token, a marker image on projection 2 might very occasionally belong to more than one of these sets, but very rarely more than two of the sets. The number of possible permutations to match marker images on the two projections is then reduced from $n!$[13] to 2^m, where $m \ll n$.

For each of the permutation of pairings among marker images (i.e., each match of marker images), we computed the 3-D locations of the markers, which was taken to be midway between the closest approach of the rays of matched marker images. The rotation and translation needed to bring the set of markers back to the known positions of the markers of the reference films was calculated by minimizing the sum of squares of the distances between corresponding markers of the two sets. The translation that minimized this sum was the translation of the centroid of the markers. The rotation about the centroid that minimized this sum of squares was determined by a downhill simplex method.[14] The combination that gave the smallest sum of squares after transformation was taken to be the right match of marker images. The corresponding transformation defined the translations and rotations needed to correct for the setup error.

3. Methods of data analysis

The positions of the markers after they were transformed back were also recorded. Due to finite precision in locating marker images on film and the precision in setting up the imaging geometry for the exposure of the films, the computed locations of the markers after the phantom was computationally transformed back to the reference position did not coincide exactly with their expected locations at the reference position.[15] The precision in locating the markers in 3-D was quantified by the standard deviations of the coordinates of markers about their expected locations at the reference position. The average position vector of a marker from all film pairs after the phantom was computationally transformed back to the reference position was used as a statistical estimate of the expected location of that marker.

Surface markers and implanted markers were analyzed independently. Furthermore, within each of these two groups, separate standard deviations were calculated for markers with distinct marker images and those with at least one overlapping marker image. After the analysis of localization of markers, the transformations for realignment were computed independently for each group of markers using markers with distinct marker images only.

III. RESULTS

Out of the 756 marker images (14 marker images per film and 27 film pairs), the *general* marker recognition algorithm for the reference films located 750 marker images correctly, although 27 of them were incorrectly interpreted as overlapping images. In addition, 37 false marker images were located by the algorithm. Here 36 of the false marker images were located at air gaps between slices of the skull phantom, accounting for the bulk of the false images. An image artifact on one of the films accounted for the other false marker image.

The *more specific* algorithm used for subsequent treatment films correctly located all marker images, including overlapping images, with no false positives.

TABLE I. Standard deviation of marker coordinates from the expected locations after the phantom was computationally transformed back to the reference position. The markers were divided into four groups: (a) implanted markers with distinct images; (b) surface markers with distinct images; (c) implanted markers with overlapping images in at least one projection; (d) surface markers with overlapping images in at least one projection.

group	Lateral direction (mm)	Vertical direction (mm)	Longitudinal direction (mm)
a	0.09	0.08	0.08
b	0.11	0.13	0.06
c	0.06	0.16	0.12
d	0.11	0.26	0.08

Standard deviations of marker coordinates after the purposely misaligned phantom was computationally transformed back to the reference position are tabulated in Table I. For markers with distinct images, the precision is on the order of 0.1 mm. Comparing markers with overlapping images to those with distinct images, the standard deviation increased from 0.13 to 0.26 mm and from 0.08 to 0.16 mm in the vertical direction, for surface and implanted markers, respectively. This is consistent with the fact that the overlapping marker images in the lateral projection were displaced in the vertical direction (Fig. 1).

The computed translations and rotations required for realignment of the phantom for each misalignment were compared with the known displacements purposely set for the phantom, as indicated on the equipment. The maximum difference for translation is 1.2 mm and that for rotation is 0.38°. The results for implanted markers are shown in Fig. 3. The root-mean-square (rms) difference for vertical motion is 0.6 mm, which for longitudinal motion is 0.7 mm and for lateral motion is 0.4 mm. The rms difference for couch rotation, tilt, and roll are 0.07°, 0.08°, and 0.28°, respectively. These differences were comparable to the accuracies of the equipment used to set the displacements.

Using the estimated precision of the coordinate of individual markers, the estimated precision of the computed translations and rotations required for realignment of the phantom can also be estimated. As the coordinates of individual markers could be determined to an estimated precision of 0.1 mm, the translation of the phantom (which is quantified by the average translation of the set of markers) should be determined to a precision at least as good as 0.1 mm. If the markers are spaced more than 25 mm from their centroid, angles should be determined with a precision of ~0.004 rad (0.1 mm/25 mm); this is approximately 0.2°. The results for translations in Fig. 3 indicate differences much higher than these estimates. As mentioned above, these are thought to be mostly due to the precision with which the displacements could be read out on the equipment and not due to the methodology employed. To demonstrate this, we checked the correlation between the transformations from the implanted markers and the independently obtained transformations from the surface markers (Fig. 4). The rms differences for vertical,

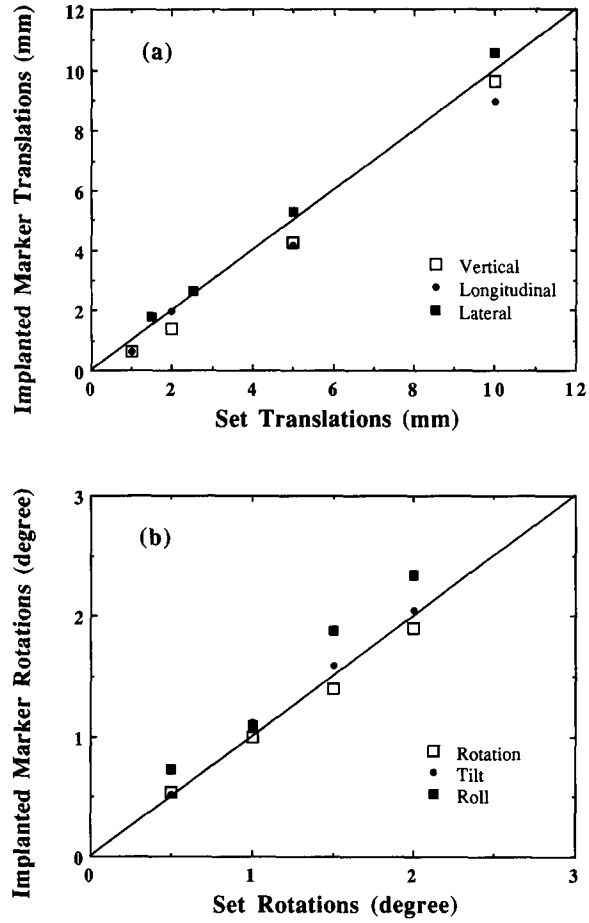

FIG. 3. Accuracy of the method used to determine phantom misalignment. Computed transformations for patient realignment are plotted against phantom displacements purposely set (as indicated by the equipment). The straight line on the plots indicates perfect accuracy (i.e., computed values=set values). (a) Translations using markers implanted inside the phantom. (b) Rotations using markers implanted inside the phantom.

longitudinal, and lateral translations were only 0.08, 0.07, and 0.06 mm, respectively, and rms differences for rotation, tilt, and roll also dropped to 0.1°, 0.07°, and 0.13°, respectively. Additionally, except for four cases (1.0 cm vertical translation, 1.5° and 2.0° rotation, and 0.5° roll), all data points in Fig. 4 were obtained with only four markers in either the set of implanted markers or the set of surface markers, because only markers with distinct marker images were used to obtain the transformations. In all, this implies that (a) comparable precision can be obtained with implanted markers and surface markers; (b) the precision that can be obtained is better than or comparable to the equipment used to set the displacements; and (c) it is not necessary to have more than four markers to achieve this level of precision.

IV. DISCUSSIONS

Results of this study demonstrate that the precision and accuracy of the computed translation and rotation is adequate for clinical applications. In the clinic, radio-opaque markers made of tissue compatible material can be im-

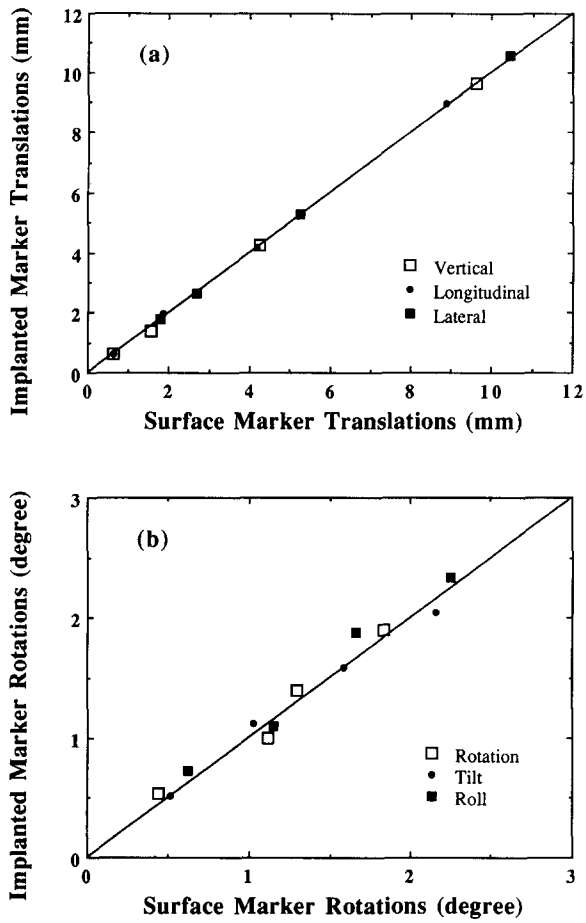

FIG. 4. Correlations between displacements computed from markers implanted inside the phantom and that from markers on the surface of the phantom: (a) translations; (b) rotations.

planted inside the patient.[16] Ideally, the markers should be implanted to the organ that we want to assure accurate positioning, such as tumor, and/or bony anatomy. On the first treatment, a pair of localization images will be obtained. Each of these images will be taken with a specific rectangular field covering the markers. If the treatment fields include at least two fields from nonparallel directions, and all markers are within the treatment field, localization images of the treatment field can be employed. The rectangular jaw edges transmitting through the custom blocks can be used to determine the coordinate system. The markers will be localized in 3-D space using the general algorithm. During subsequent treatments, the same pairs of localization images are obtained. The translation and rotation needed to reposition the patient are computed using the specific algorithm. Patient motion between the time when localization images are taken, and the actual treatment cannot be taken into account by this technique.

In the present study, film was used to acquire the images. The films were processed manually and they were loaded into the film digitizer manually. The whole procedure can be fully automated if an electronic portal imaging device is available.

In the experiment, portal images were employed as the reference images to avoid the systematic error between setting up the phantom on the simulator and the linac. Other candidates for reference images are x-ray film images taken with a diagnostic x ray (either on a simulator or on a treatment unit with a diagnostic x-ray tube), and digitally reconstructed radiograph (DRR) from CT images. Film images taken with a diagnostic x ray has much higher contrast and has better resolution. CT images usually have slice thicknesses between 0.5 to 1.0 cm. The resolution in the slice thickness direction will be inferior.

As mentioned above, the general algorithm used here for the reference images was based on a similar algorithm used for mammography, and we expect it to be equally applicable to diagnostic x-ray images after adjustment of parameters. However, we do not expect the general algorithm to be applicable to DRR's due to its inferior spatial resolution. For the specific algorithm, the reference images serves three purposes (1) to generate a template for the shape, size, and contrast of a marker image; (2) to generate a template for the location of marker images to determine ROI's, and (3) to generate the reference 3-D locations of markers. Diagnostic x-ray images and DRR's are not useful for the first purpose. However, we expect the template of the marker images to be relatively independent of patient and generic templates for marker images at different clinical sites can be generated after enough clinical experience has been accumulated. Since diagnostic x-ray images have been used extensively for the localization of radioactive seeds in brachytherapy, they will provide precise positions for the second and third purpose. DRR's and CT will probably be able to achieve the precision in position for the second purpose, but they will be marginal in providing the reference 3-D locations of markers.

In the computations, the markers were assumed to be attached to a rigid body. In practical situations, the patient is not rigid, and there may be relative motion among the markers. When the transformation is not a rigid body transformation, the method gives a least squares estimate to the solution (the sum of squares of the distances between the markers of the corrected setup and the reference setup is minimized). The minimized sum of squares will also give an estimate of the deviation from the rigid body approximation. Clinical tests need to be performed to check the applicability of the least square solution.

Moreover, the patient is assumed to be stationary between the two projections. If the patient moves between the two projections, the minimum distance between the rays joining the x-ray source locations, and a marker of the two projections will be increased. The algorithm currently sets an upper limit of 2 mm on the minimum distance, which is also the limit that is used in our treatment planning system for brachytherapy source localization. Clinical tests will be needed to evaluate the applicability of the 2 mm upper limit, and also the validity of the stationary patient assumption.

A skull phantom was employed in the study and the performance of the algorithm has not been tested on images of other anatomical sites. As the skull is one of the body parts that has more complicated image features on

film, it is expected that the algorithm will be comparably effective on films of other sites. For the general method of locating marker images, only the false positive from the image artifact on one of the films is significant, since patients are not layered with air gaps between slices and markers can be arranged so that they do not have overlapping images. Clinically, there are patients with surgical clips and other artifacts such as air cavities and bubbles. Usually, the contrast of surgical clips is much less than air gaps that we have seen here. Air bubbles can be very similar in shape to our markers. Since air bubbles appear as dark circles and our markers are white circles, we believe that air bubbles can be effectively removed by the grey scale thresholding stage of the algorithm. However, the effectiveness of the image processing algorithm on clinical images needs to be studied.

The routines used here were written to test the algorithm and were not optimized for speed. The time required to process one pair of films using the general algorithm was about 8 min on a VAX station 3520 without parallel processing codes. The specific algorithm needs 1.5 min per marker on the same computer. A large proportion of the time was spent on convolution for the general algorithm and on computing the correlation function for the specific algorithm. Both were done in the spatial domain instead of the frequency domain. If Fast Fourier Transform and faster computers or special hardware for convolution were used, computation speed is expected to increase by orders of magnitude.

Clinical treatment machines currently available do not have patient couches that can be moved in six degrees of freedom. Conventional couch designs allow translation in three orthogonal axes and rotation about a vertical axis. However, the calculated transformation to correct for setup errors can, in principle, still be implemented with conventional equipment by adding rotation of the gantry and collimator to the translations and rotation of the couch above; thus repositioning the patient at the desired position relative to the beam. However, the correction for a small error sometimes involves major motion of the gantry, collimator, and table. For example, suppose that a supine patient is to be treated with an anterior–posterior field and a lateral field, but the patient is inadvertently set up tilted, such that the head is slightly too high and the toe is too low. To correct for this setup error, the lateral field would simply require a slight rotation of the collimator to account for the patient tilt. But, to correct the patient position for treatment of the AP field, both the couch and the collimator would need to be rotated by 90°, after which the gantry could then be rotated by a small angle from vertical to account for the patient tilt. In fact, the required angles of rotation of the collimator and the couch are discontinuous functions of the error at zero error in tilt. This is clearly a complicated correction for a small error in setup, and it is desirable to have a couch that can be moved in six degrees of freedom to correct for the setup error directly.

V. CONCLUSIONS

Results of this study show that radio-opaque markers can be effectively identified by image processing techniques and setup errors can be determined accurately. Both implanted markers and surface markers can provide good precision, and not more than four markers are needed. However, the results were obtained with a rigid skull phantom. Further study is necessary to assess the usefulness of such procedures for nonrigid body motions and other body sites. A new couch/table top design that directly incorporates changes in patient position in six degrees of freedom associated with a rigid body is desirable for use in automated patient setup correction.

APPENDIX: EFFECT OF GRAY SCALE TRANSFORMATION ON CONTRAST OF MARKER IMAGES

The decrease in dose E behind a small low contrast object such as a marker is

$$\Delta E \sim E_p \mu \tau,$$

where E_p is the dose due to primary x ray, μ is the linear attenuation coefficient and τ is the thickness of the marker. Let S be the scatter to primary ratio, $\Delta E = E\mu\tau/(1+S)$. $\Delta E/E$ will be constant if we assume that the scatter to primary ratio is constant. Let the optical density D and exit dose E be related by $D=f(E)$, and let $T(D)$ be the gray scale transformation applied to D, i.e., $D^*=T(D)$. We may define g, such that $D^*(E)=g(E)$. Then the contrast ΔD^* can be approximated by

$$\Delta D^*(E) \sim g'(E)\Delta E = (\Delta E/E)Eg'(E).$$

If we require ΔD^* to be constant, then $Eg'(E)=\text{const}$ or $g(E)=a\ln(E)+b$. Substituting T for g and D for E, we have

$$T(D)=a\ln[f^{-1}(D)]+b.$$

If $D=cE$ where c is a constant, then $f^{-1}(D)=D/c$ and

$$T(D)=a\ln(D)+[b-a\ln(c)].$$

Therefore, with logarithmic gray scale transform, ΔD^* is constant for all markers if the scatter to primary ratio is constant and the response of the recording medium is linear. For metal-screen-film systems and most electronic portal imaging systems, linear response is a good approximation. The scatter to primary ratio S for megavoltage x-ray beams is usually less than 0.5 so that $(1+S)$ and ΔD^* will not vary by much more than 50% over the image.

[1]I. Rabinowitz, J. Broomberg, M. Goitein, K. McCarthy, and J. Leong, "Accuracy of radiation field alignment in clinical practice," Int. J. Radiat. Oncol. Biol. Phys. **11**, 1857–1867 (1985).

[2]S. Blanco, M. A. Lopez-Bote, and M. Desco, "Quality assurance in radiation therapy: Systematic evaluation of errors during the treatment execution," Radiotherapy Oncol. **8**, 256–261 (1987).

[3]K. J. Halverson, T. C. Leung, J. B. Pellet, R. L. Gerber, M. S. Weinhous, and J. W. Wong, "Study of treatment variation in the radiotherapy of head and neck tumors using a fiber-optic on-line radiotherapy imaging system," Int. J. Radiat. Oncol. Biol. Phys. **21**, 1327–1336 (1991).

[4]J. Bijhold, M. van Herk, R. Vijlbrief, and J. V. Lebesque, "Fast evaluation of patient set-up during radiotherapy by aligning features in portal and simulator images," Phys. Med. Biol. **36**, 1665–1679 (1991).
[5]J. M. Balter, C. A. Pelizzari, and G. T. Y. Chen, "Correlation of projection radiographs in radiation therapy using open curve segments and points," Med. Phys. **19**, 329–334 (1991).
[6]S. M. Jones and A. L. Boyer, "Investigation of an FFT-based correlation technique for verification of radiation treatment setup," Med. Phys. **18**, 1116–1125 (1991).
[7]R. K. Ten Haken, D. L. McShan, A. Gerhardsson, A. F. Thornton, Jr., and B. A. Fraass, "Use of radio-opaque markers in automated patient setup," Med. Phys. **16**, 678 (1989) (abstract).
[8]D. Jones, D. Christopherson, M. D. Hafermann, J. Rieke, J. Travaglini, and S. Vermeulen, "Experience with a technique for fractionated radiosurgery," Int. J. Radiat. Oncol. Biol. Phys. **19**, (Supplement 1), 134 (1990) (abstract).
[9]D. R. Haynor, A. W. Borning, B. A. Griffin, J. P. Jacky, I. J. Kalet, and W. P. Shuman, "Radiotherapy planning: Direct tumor location on simulation and port films using CT," Radiology **158**, 537–540 (1986).
[10]H. P. Chan, K. Doi, S. Galhotra, C. J. Vyborny, H. MacMahon, and P. M. Jokich, "Image feature analysis and computer-aided diagnosis in digital radiography. 1. Automated detection of microcalcifications in mammography," Med. Phys. **14**, 538–548 (1987).
[11]R. A. Kruger and S. J. Riederer, *Basic Concepts of Digital Subtraction Angiography* (Hall, Boston, MA, 1984).
[12]W. K. Pratt, *Digital Image Processing* (Wiley, New York, 1978).
[13]R. L. Siddon and L. M. Chin, "Two-film brachytherapy reconstruction algorithm," Med. Phys. **12**, 77–83 (1985).
[14]W. H. Press, B. P. Flannery, S. A. Teukolsky, and W. T. Vetterling, *Numerical Recipes* (Cambridge University, New York, 1986).
[15]K. L. Lam and R. K. Ten Haken, "Improvement of precision in spatial localization of radio-opaque markers using the two-film technique," Med. Phys. **18**, 1126–1131 (1991).
[16]H. M. Sandler, R. L. Bree, P. W. McLaughlin, H. B. Grossman, and A. S. Lichter, "Localization of the prostatic apex for radiation therapy using implanted markers," Int. J. Radiat. Oncol. Biol. Phys. **27**, No. 4 (1993).